Langmuir-Blodgett Films

J. A. Zasadzinski,* R. Viswanathan, L. Madsen, J. Garnaes, D. K. Schwartz

The controlled transfer of organized monolayers of amphiphilic molecules from the air-water interface to a solid substrate was the first molecular-scale technology for the creation of new materials. However, the potential benefits of the technology envisioned by Langmuir and Blodgett in the 1930s have yet to be fully realized. Problems of reproducibility and defects and the lack of basic understanding of the packing of complex molecules in thin films have continued to thwart practical applications of Langmuir-Blodgett films and devices made from such films. However, modern high-resolution x-ray diffraction and scanning probe microscopy have proven to be ideal tools to resolve many of the basic questions involving thin organic films. Here, studies are presented of molecular order and organization in thin films of fatty acid salts, the prototypical system of Katharine Blodgett. Even these relatively simple systems present liquid, hexatic, and crystalline order; van der Waals and strained layer epitaxy on various substrates; wide variations in crystal symmetry and interfacial area with counterions; modulated superstructures; and coexisting lattice structures. The wide variety of possible structures presents both a challenge and an opportunity for future molecular design of organic thin-film devices.

The trend in new materials has been increasingly toward the more sophisticated control of chemical specificity and physical dimensions. High-tech acronyms such as MBE (molecular beam epitaxy), MOCVD (metal organic chemical vapor deposition), and LPE (liquid phase epitaxy) describe some of the ways available to create new materials by the modification of a substrate with a thin layer or layers. Although not usually grouped with these techniques, the transfer of organized monolayers of amphiphilic molecules from the air-water interface to a substrate [commonly known as the Langmuir-Blodgett (LB) technique, with materials known as LB films] was the first of the molecular-scale materials technique (*1*, *2*). However, the controlled fabrication of molecular films was a novelty 60 years ago, because there was no need for such highly evolved molecular architectures (*1*). With the current demand for materials with tailored interfacial properties, LB technology should be reevaluated as a future component of "molecular engineering." Of course, as in all thin film techniques, limitations exist: LB films are restricted to amphiphilic molecules capable of forming monolayers at a liquid-vapor interface.

The films produced by LB deposition have many of the same potential applications in optical and electronic devices as do thin films produced by MBE or CVD (*1–4*). The richness of chemical functionality made possible by novel organic synthesis makes organic thin films a likely area for future advances as the limitations of single crystal forms of elements such as silicon and germanium become more apparent (*1–4*). Because living cells are made up of many of the same materials as LB films (fatty acids, phospholipids, and proteins), excellent potential also exists for the development of compatible interfaces between conventional materials and biomaterials to create biosensors or biochemical probes (*4*). Organic thin films have also been used as templates to grow oriented crystals of proteins (*5*) or inorganic materials (*6*) and can often alter crystalline habits or growth kinetics, as in biomineralization (*7*) or the formation of zeolites (*8*).

In the conventional scheme of the LB technique (Fig. 1), the monolayer organization on water is expected to be transferred relatively unchanged to the substrate (*1*, *2*). However, x-ray scattering (*9*), phase behavior, and fluorescence (*10*) and Brewster angle optical microscopy (*11*) have provided sufficient information that monolayer structure at the air-water interface can be compared to LB film structure on substrates as determined by electron diffraction (*12*), x-ray diffraction (*13–15*), and scanning probe microscopy techniques (*16–41*). These studies have shown that the relation is not as simple as was hoped. LB film structure is influenced by a number of factors that are different from those that govern structure in Langmuir monolayers. As a result, current research is being focused on how molecular organization evolves during transfer and subsequent stages including drying and annealing to predict how chemical perturbations, the number of layers, the proximity to the substrate or free surface, and the chemical environment influence the structure, growth, and stability of the LB films. Several books and reviews are available that describe the state of the art of LB films up to about 1990 and provide an excellent background on LB film deposition, characterization, applications, and history (*1–4*).

Since 1990, scanning probe microscopy has helped to resolve many long-standing questions about LB films. For example, one of the major impediments to applications has been the lack of a routine method to assess film quality nondestructively on the nanometer scale. Although LB films have been extensively studied by spectroscopy and x-ray and electron diffraction (*1–4*, *12–15*), these techniques are not sensitive to defects such as pinholes or tears within layers. Film defects have been examined with optical or electron microscopy but only at low resolution; such techniques usually result in destruction of the films (*42*). Atomic force microscopy (AFM) (*16–18*), on the other hand, has turned out to be a nearly ideal, nondestructive, high-resolution method to investigate LB film structure and defects at length scales from <0.1 nm to >10 μm (*19–41*). Hence, it is

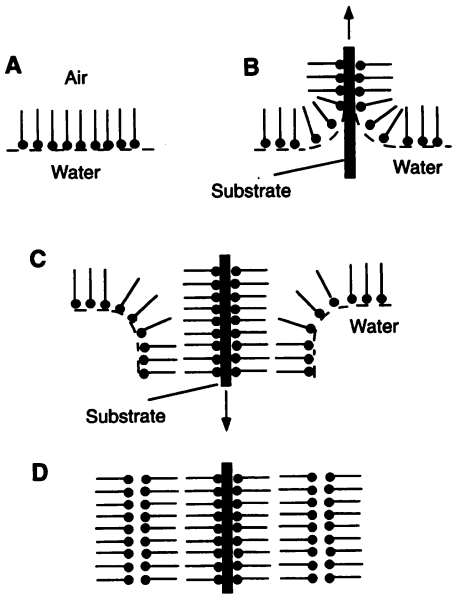

Fig. 1. Conventional schematic of the LB technique. In the first step (**A**), a suitable amphiphilic molecule is dissolved in a volatile solvent that is then spread at the air-water interface to form a Langmuir monolayer. With a barrier, the area of the trough can be altered to change the local density of the molecules, and usually the local organization and order as well. The structure of the monolayer has been extensively studied (*10*). To form the LB film (**B**), a substrate is passed through the interface a given number of times, with each pass adding another monolayer to the LB film (**C** and **D**).

J. A. Zasadzinski, R. Viswanathan, and L. Madsen are in the Department of Chemical and Nuclear Engineering, University of California, Santa Barbara, CA 93106, USA. J. Garnaes is at the Danish Institute of Fundamental Metrology, Lundtoftevej 100, DK-2800 Lyngby, Denmark. D. K. Schwartz is in the Department of Chemistry and Biochemistry, University of California, Los Angeles, CA 90024, USA.

*To whom correspondence should be addressed.

now possible to characterize the structure of LB films quickly and reliably with AFM and to use this information as feedback to improve film quality. In addition to quality control, high-resolution studies of LB films can provide a wealth of information on the structure of condensed phases of complex molecules. A variety of LB films have been investigated with AFM, including lipid and protein films (*25–28*), polymer films (*25, 29–31*), and specially functionalized molecular films (*25, 32–34*). The atomic force microscope can also investigate the local frictional and elastic properties of the films with nanometer resolution (*41*).

Here, we present work done on prototypic LB films made from saturated fatty acids. These films have been the workhorses of both research and applications since the days of Langmuir and Blodgett (*1*). However, fatty acid films are far from simple. They exhibit a complex assortment of structure and organization including amorphous, hexatic, and crystalline in-plane order (*18–25, 35–40*); systematic trends in interfacial density (*36–40*); in-plane lattice spacings and positional correlations that are coupled to the number of layers of and the proximity to the substrate (*37, 38*); multiple lattices coexisting in the same layer (*36, 37, 40*); the spontaneous symmetry breaking of achiral molecules into chiral lattices (*36, 39*); and stable, periodic defect structures that arise from competition between preferred head and tail lattice spacings (*21, 23, 36, 37, 39, 40*). Lattice defects such as dislocations (*18, 24*) and grain boundaries (*21, 23, 33*) can also be studied, and their effects on film applications can be assessed. LB film stability can also be addressed in realistic environmental conditions (*20*). To further the applications of LB films in technology requires a good understanding of how complex molecules fit together and what type of order within the layers, between the layers, and between the substrate and the film is best suited to a particular application. This understanding might also lead to better design criteria for synthesizing the molecules themselves (*43*).

Effect of Competing Length Scales and Symmetry on Molecular Packing

The amphiphilic molecules in LB films incorporate disparate chemical functionalities in their hydrophobic "tail groups" and hydrophilic "head groups." These varied functionalities lead to competing interactions and conflicts between the packing requirements of the heads and tails (*40*). Atomic force microscopy studies of fatty acid salts have shown that the interfacial area per molecule is controlled by the interaction of the counterion with the carboxylic acid head group, or more generally, by the area or bonding requirements (or both) of the head group (Table 1). After the interfacial area is set by the head group, the alkane tails pack in such a way as to maximize the van der Waals contact (equivalent to maximizing the alkane density), usually in ways similar to bulk alkane lattice configurations (*44*). For example, the lattice parameters, area per molecule, and symmetry of lead stearate and cadmium aracidate (CdA_2) films (*37*) are nearly identical to those of bulk polyethylene (*44–46*). In many of the more complex molecules used to make LB films, a significant portion of the tail group is a straight chain, saturated alkane (*1, 2*), and the organization of the films will quite likely be determined by a competition between the alkane packing constraints relative to the rest of the molecule (*46*). This extension to more complex molecules is somewhat simplified by the fact that palmitate (P), stearate (St), arachidate (A), and behenate (B) lattices (C_{16} to C_{22}) are identical for a given head group. By an understanding of the relation between the alkane packing requirements and the size and shape of the functional group necessary for a particular application, more reasoned choices can be made as to molecular design (*43*). These studies should also be compared to Monte Carlo and molecular dynamics simulations of alkane packing as a function of interfacial density (*45, 46*).

As can be seen from Table 1, the interfacial area per molecule is well correlated (except for zinc) with the degree of ionic versus covalent bonding as determined by the difference between the electronegativities of the carboxylic acid oxygen [about 3.5 (*47*)] and of the various counterions. An electronegativity difference greater than 2 suggests ionic bonding, while a difference less than 2 suggests covalent bonding (*47*). Surface potential measurements on Langmuir monolayers (*48*) show that the alkaline earth metals (Ba, Ca, and Mg) interact with fatty acids electrostatically by the screening of negative charges in a nonspecific way, while Cd, Mn, and Pb interact more specifically by covalent bonding (*49*). The effect of pH on isotherms shows a similar trend. Both Cd and Mn effectively remove the "liquid condensed" phase in monolayer isotherms over a pH range of 6 to 7, which is consistent with the estimated pK_a (acidity constant) of the fatty acid film of about 5.6 (*48, 50*). Langmuir-Blodgett films of CdA_2 show complete saturation of the carboxylic acid with Cd at a pH $\geq$6.5 (*50*). Lead affects the monolayer at significantly lower pH, with the liquid condensed phase in monolayer isotherms absent at pH > 4 (*48*), and completely saturates the carboxylic acid in LB films at pH $\geq$4.5 (*50*). Barium, calcium, and magnesium fatty acid LB films do not fully saturate until pH 8.5 (*50*).

Although the interfacial area of the molecule changes by more than 20% between ions, the alkane chain density cannot change by this amount and maintain a crystalline lattice. The minimum cross-sectional area of a saturated alkane in a condensed phase is about 18 Å^2 (*51*). As the interfacial density decreases, the alkane chains can tilt to maintain close to their bulk density (*46*). By tilting, the chain lattice, in principle, can become compatible with any imposed molecular area without significantly changing the van der Waals contact of the chains (*46*). A simplified cylindrical molecule whose head group prefers a separation β and whose tail group prefers a separation α (with $\alpha < \beta$) will tilt at an angle θ such that $\cos\theta = \alpha/\beta$ (*40*). However, the tetrahedral coordination of the alkane backbone leads to a zigzag pattern of the methylene units and a roughly elliptical shape, with the major axis along the zigzag direction (*44, 52*). Hence, the alkane chains can pack together only at certain discrete tilt angles to maintain maximum contact (*44, 52*). The allowable packings of alkanes become an exercise in geometry, and we have consistently observed two of the highest density lattice structures predicted by Kitaigorodskii: the

Table 1. Lattice structures of fatty acids with different counterions.

Counterion	Layers*	Local lattice	Tilt (direction†)	Molecular area (Å^2)	Electronegativity‡
Pb	7	Herringbone	0°	17.9	1.8
Cd	3	Herringbone	0°	18.0	1.7
Mg (4 by 2)	3	Herringbone	0°	18.7	1.3
Mg (2 by 2)	3	Triclinic	0°	18.7	1.3
Mn	5	Herringbone	19° (NNN)	19.5	1.5
Ca	3	Triclinic	26° (BN)	19.6	1.0
Ba (2 by 2)	3	Herringbone	19° (NNN)	20.2	0.9
Ba (3 by 1)	3	Triclinic	26° (BN)	20.4	0.9
Zn	7	Hexagonal	33° (NN)	22.2	1.6

*Number of layers to reach a consistent lattice structure on a mica substrate. †Tilt directions are NN, toward nearest neighbors; NNN, toward next-nearest neighbors; and BN, between nearest and next-nearest neighbors. ‡Electronegativity should be compared to oxygen's value of 3.5 in the assessment of the relative ionic or covalent nature of the bond.

herringbone and the triclinic packings (Fig. 2) (*44*). However, even with the various lattice structures and allowable tilts, an alkane lattice cannot accommodate any arbitrary molecular area. This limitation can lead to defects and modulated structures when the competition between length scales is sufficient (*40*) and can even lead to situations in which, for certain areas per molecule, more than one lattice structure is observed (*36–39*).

Molecular resolution images of LB films of CdA_2, MnA_2, and $PbSt_2$ are shown in Fig. 3, A, B, and C, respectively, along with their two-dimensional Fourier transforms (FTs) (*53*). The lattice symmetry of these three films is the same, as the FTs show a rectangular lattice with alternating bright and dim spots. The small but finite intensity of the dim Fourier spots proves that the unit cell consists of two molecules. Given the particular dimensions measured, the real space lattice structure corresponds to a two-molecule unit cell with a herringbone packing [called the "*R*" subcell by Kitaigorodskii (*44*)]. In the herringbone packing, the zigzag or long axis of adjacent molecules alternates to facilitate close packing (Fig. 2). The measured CdA_2 and $PbSt_2$ lattices are similar to those of the "ideal" untilted cell dimensions of 0.496 by 0.742 nm as predicted by Kitaigorodskii (*44*). The lattice parameters measured by AFM are very similar to that observed for thick films of $PbSt_2$ (*13*) and thin films of CdA_2 (*14*) as measured by x-ray diffraction. The measured MnA_2 lattice is close to the ideal tilted (19° in the next-nearest neighbor direction) cell dimensions of 0.496 by 0.785 nm (*44*). This ideal tilt of 19° is based on the idea that alkyl chains prefer to tilt at certain specific angles such that the chain packing in the plane perpendicular to the chains is undisturbed (*44, 52, 54*).

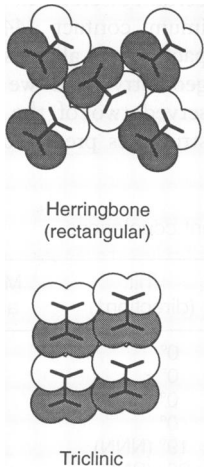

Fig. 2. Crystalline alkanes have several distinct forms of close packing. As viewed along the direction normal to the chains, the most commonly observed packings are the herringbone and the triclinic. The dark lines represent the zigzag of the carbon backbone, and the circles represent the van der Waals radii of the hydrogen. Different shadings represent hydrogens attached to adjacent carbons; that is, the more lightly shaded hydrogens might be attached to the tenth carbon in a chain while the darker ones are attached to the ninth carbon, therefore below the light ones. The triclinic packing does not have a plane of mirror symmetry and is inherently chiral.

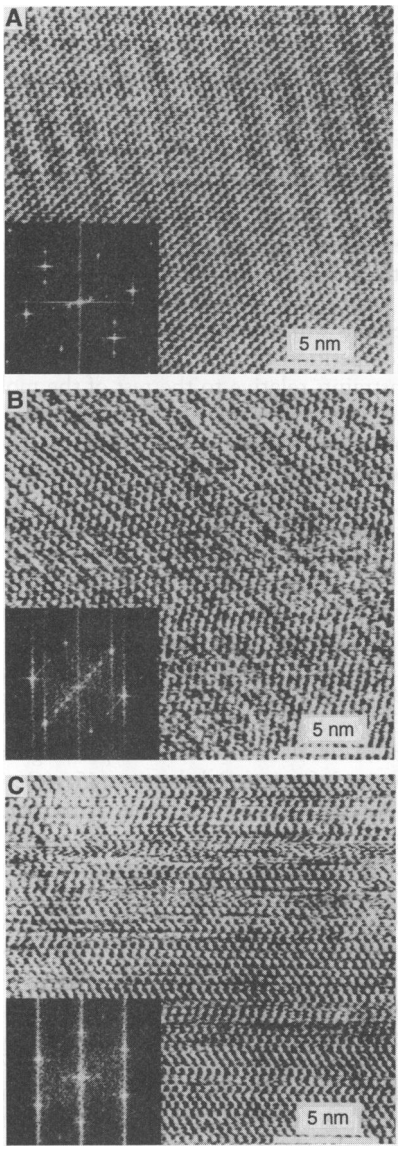

Fig. 3. Images (20 nm by 20 nm) of LB films of various fatty acid salts. Lighter colors correspond to higher areas, and the peak to valley height modulation is ~0.2 nm. The respective two-dimensional FTs are inset. The vertical and horizontal streaks in the FTs are the result of noise from the raster pattern of the AFM. (**A**) Three-layer CdA_2 on mica. The FT shows the rectangular reciprocal lattice indicative of the herringbone packing. The two bright inner spots (in the nearly horizontal direction) correspond to the periodic height modulation along the [10] direction, which is visible as light and dark stripes in the image. (**B**) Three-layer MnA_2 on mica. The FT shows the rectangular herringbone lattice reflections; however, the positions of the spots are consistent with a molecular tilt in the next-nearest neighbor or [10] direction. The additional spots correspond to a periodic height modulation with a period of about 1.2 nm. (**C**) Three-layer $PbSt_2$ on mica. $PbSt_2$ does not show any periodic height modulation.

The structures coexisting in a single BaA_2 film are shown in Fig. 4 (*36*). The predominant structure (~70% of the surface area) is a 26° tilt, triclinic packing with regular stacking faults every third molecule resulting in a "sawtooth" surface modulation and a three-molecule, 3 by 1 unit cell of area 61.1 Å^2 (20.4 Å^2/mol) (*36*). The minority structure (<10%) is a four-molecule, 2 by 2 unit cell of area 80.7 Å^2 (20.2 Å^2/mol) in which pairs of molecules are packed in a tilted (19°) rectangular herringbone lattice (similar to MnA_2), but adjacent rows alternate vertically up and down by a single methylene group. The difference in molecular area between the two lattices is <1%. A disordered third structure, which occupies 20 to 30% of the film area, presents only diffuse spots in the FTs and has close to the same area per molecule as the two crystalline structures. These three coexisting structures indicate that the counterion sets the molecular area, while the alkane lattice adjusts to find an optimal packing, given this con-

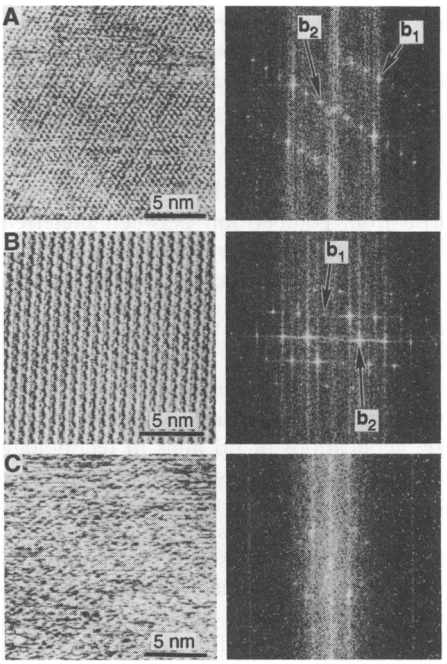

Fig. 4. (**Left**) Molecular resolution images and (**right**) FTs of the three lattice structures coexisting in BaA_2 films. (**A**) Lattice 1. A sawtooth superstructure is seen every three rows. The FT is shown with the basis of the reciprocal lattice labeled. The lattice spacings are consistent with a triclinic packing with a regular stacking fault every three molecular repeats. (**B**) Lattice 2. Alternating rows of high and low zigzag molecules can be seen clearly. The FT shows that the local packing is similar to that of MnA_2 (Fig. 3B): a herringbone packing with a tilt in the next-nearest neighbor direction. (**C**) Disordered isolated areas of molecular order are visible but without long-range correlation. The FT shows that the peaks are diffuse because of short-range order. In all three lattices, the area per molecule is nearly identical.

straint. For the larger molecular areas, several packings can apparently have the same density and similar free energies. However, these coexisting structures are metastable; upon annealing, the triclinic structure is preferred (55).

Calcium arachidate adopts only a triclinic lattice. However, because of the molecular and packing anisotropy, the triclinic packing is chiral, leading to both left-handed and right-handed packings (Fig. 5, A to C). As can be seen in Fig. 5, B and C, which are from two different crystalline domains in the same film, the six brightest spots in the FTs form a skewed hexagon and correspond to three different spacings of (a) 0.442 nm, (b) 0.576 nm, and (c) 0.686 nm. The FT has no axis of mirror symmetry; hence, the real space CaA_2 lattice also has no mirror symmetry and is chiral, although the constituent molecules are achiral. Figure 5C is the FT of Fig. 5A and has the same progression (clockwise, abc) of lattice spacings. Figure 5B is the mirror image of Fig. 5C and has the same lattice spacings, but the progression (clockwise) is acb. The molecules tilt along a direction between nearest and next-nearest neighbors by 26° from the surface normal, as determined by the measured bilayer thickness of 5.0 nm, which also adds to the chirality (56). The observed tilt is consistent with FT infrared and near-edge x-ray absorption fine structure measurements that show CaA_2 monolayers to be tilted (52, 57). Atomic force microscopy images also show that racemic mixtures of chiral molecules can be spontaneously resolved into left-handed and right-handed domains in LB films (34).

A $MgSt_2$ film in which two distinct lattice structures are present and meet at a grain boundary is shown in Fig. 6. As in BaA_2, one of the structures is based on a locally triclinic structure (2 by 2), while the other is based on a herringbone packing (4 by 2). The FTs of each domain show the dominant symmetry. The AFM images also show that the order in the film is preserved nearly to the grain boundary, which is also the case for grain boundaries in CdA_2 films (23). In both $MgSt_2$ packings and in CdA_2, the molecules are untilted; hence, the molecules in different grains can pack closely, and the grain boundaries are very narrow. For tilted packings, however, the grain boundaries can extend over several molecular repeats (33). The preference for alkaline earth metal films to pack into triclinic lattices and for the more covalent metals to pack into herringbone lattices suggests that the local bond angles or type of bond may be important (52). In other words, the molecular areas of Ca and Mn salts are very similar, and Mg actually has a smaller area per molecule than does Mn (Table 1).

Multilayer films of ZnA_2 have a completely different structure from that of any other film we have examined. Figure 7 is an image of a seven-layer film with the FT inset. The lattice parameters determined from the FT, and the bilayer thickness of 4.6 nm, are consistent with a simple hexagonal packing with a nearest neighbor distance of 0.47 to 0.48 nm and a tilt of 33° in the direction of a nearest neighbor. This

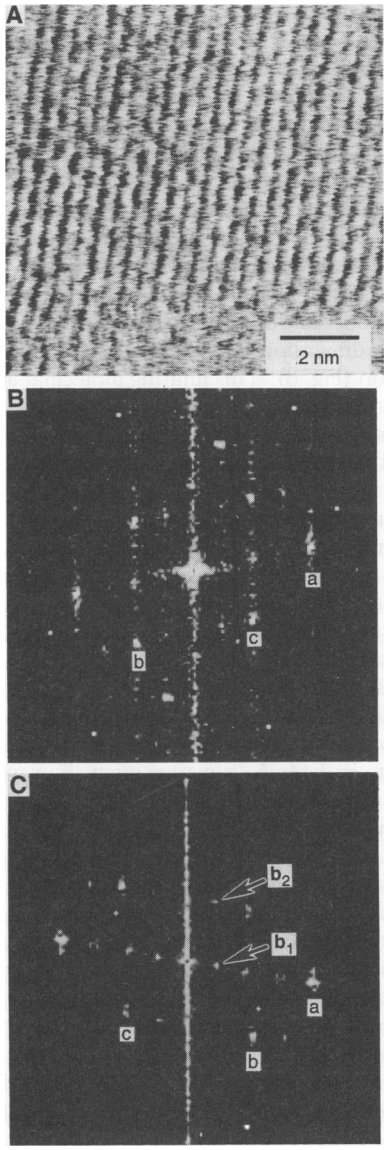

Fig. 5. (**A**) Atomic force microscopy image (10 nm by 10 nm) of trilayer LB film of calcium arachidate. The molecular rows in the film are clearly visible, along with evidence of periodicity along the rows. The six strongest reflections in the FT form a skewed hexagonal pattern with three distinct lattice repeats of (a) 0.442, (b) 0.576, and (c) 0.686 nm. The asymmetric pattern is indicative of a local triclinic packing. (**B** and **C**) Mirror-image FTs of two different domains on a single LB film of CaA. The sequence of lattice spacings in (C) is abc, whereas the sequence in (B) is acb, although the lattice dimensions are identical. The two FTs are not superimposable by any rotation within the plane of the image. The arrows pointing to b_1 and b_2 show the reciprocal lattice vectors corresponding to the 4 by 2 unit cell of CaA.

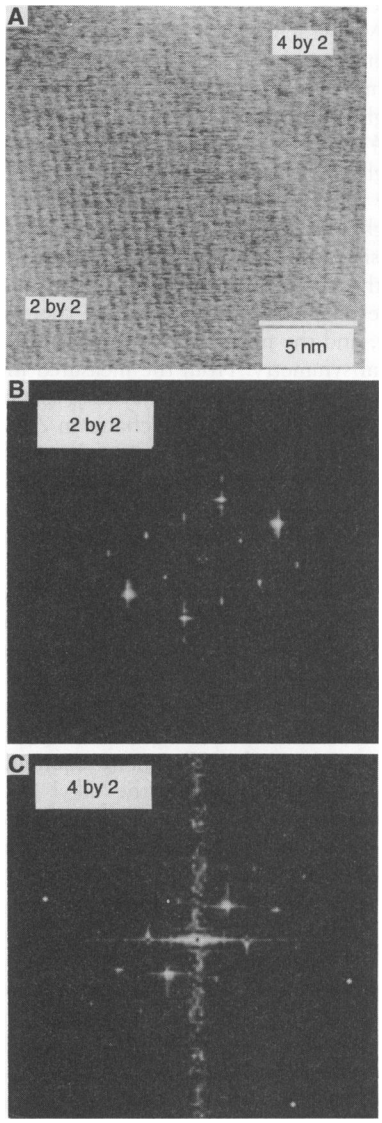

Fig. 6. (**A**) Image and (**B** and **C**) FTs of distinct lattice structures in a trilayer film of $MgSt_2$ meeting at a grain boundary in a film. In the lower left corner of (A), the FT (B) is consistent with a local triclinic packing with a 2 by 2 unit cell formed by a regular set of stacking faults. In the upper right corner of (A), the lattice structure is visibly different and the FT (C) is consistent with a local herringbone packing with a 4 by 2 unit cell formed by the alternation up and down of offsets of the molecules along the chain axis. Both structures have the same interfacial area, indicating that the counterion sets the local interfacial density and that the alkane chains then pack to maximize contact, given this density. As in BaA_2 films, there can be more than one alkane packing for a given interfacial area. The AFM images also show that the coexisting lattices match nicely, because the films are well ordered up to the grain boundary, which is no more than a few molecules wide.

packing is unusual for two reasons: The hexagonal lattice suggests that the alkane molecules have lost their elliptical shape, and the molecules are less densely packed than in either the herringbone or triclinic structures. Each alkyl chain in $PbSt_2$ and CdA_2, which, according to our previous arguments about electronegativity, should be most similar to ZnA_2, has four nearest neighbors that are relatively close, about 0.44 to 0.45 nm away, and two nearest neighbors at a distance of about 0.48 nm. The ZnA_2 packing, in which all of the neighbors are close to 0.48 nm apart, is consistent with the *R2* rotator phase (*58*); in the rotator phases, the alkane chains have much freer rotation about their long axis, and the molecules have a more cylindrical symmetry. From the measured interfacial density and tilt, the cross-sectional area perpendicular to the chains in ZnA_2 is about 19 $Å^2$, which indicates a density 5 to 6% lower than in CdA_2 or $PbSt_2$.

Substrate Effects

For all counterions, with the exceptions of lead and manganese on mica, monolayer films were disordered and showed no lattice structure. The "bulk" lattice structure for Cd, Mn, Ba, Ca, Pb, and Mg appeared after the deposition of an additional bilayer to form a trilayer film. The main requirement for long-range order in the alkyl chains seems to be an underlying head group–head group interface. This structure appears to stabilize the alkane lattice in its close-packed configuration by ions bridging between and within the layers. The substrate or the free surface does not appear to have a significant effect on the local structure other than breaking the bilayer symmetry and, hence, the coupling between adjacent headgroups (*18*).

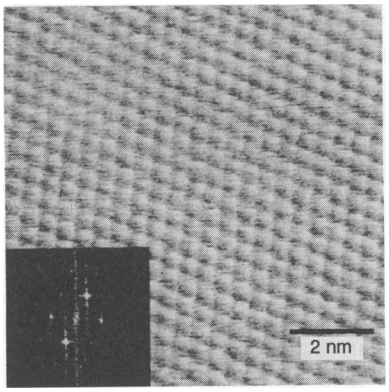

Fig. 7. Molecular resolution image (10 nm by 10 nm) and FT (inset) of a seven-layer film of ZnA_2 on mica. The lattice parameters determined from the FT, and the bilayer thickness of 4.6 nm, are consistent with a simple hexagonal packing with a nearest neighbor distance of 0.47 to 0.48 nm and a tilt of 33° in the direction of the nearest neighbors. This unusually symmetric packing is consistent with the *R2* rotator phase structure (*50*). In the rotator phases, the alkane chains rotate about their long axis and are more cylindrically symmetric, and the molecules are less densely packed than in either the herringbone or triclinic lattices.

However, monolayers of $PbSt_2$ deposited on mica have long-range order while monolayers of MnA_2 on mica show a distinct but short-range positional and long-range orientational order (*38*). Otherwise identical $PbSt_2$ and MnA_2 monolayers are disordered on amorphous oxidized silicon. Monolayers of $PbSt_2$ and MnA_2 on mica have a significantly larger lattice spacing and molecular area than do the corresponding multilayers on mica, indicating a strong coupling to the mica lattice (Fig. 8). However, by layer 7, the $PbSt_2$ lattice on mica has relaxed to the same dimensions as the three-layer film on silicon (Fig. 8). This limiting molecular area was the same as that of 100-bilayer-thick films as measured by x-ray diffraction (*13*).

Two types of epitaxy, strained layer and van der Waals, have been observed in layered materials because of film-substrate interactions. In strained layer epitaxy, the first monolayer of an adsorbed film, which has a bulk lattice constant no more than a few percent different from that of the substrate, replicates the in-plane structure of the substrate exactly, and subsequent layers gradually relax to the bulk structure of the adsorbate by incorporating dislocations. For $PbSt_2$ and MnA_2 films on mica, however, the bulk crystal structure is significantly mismatched with the substrate in both lattice constants and lattice symmetry (mica has a hexagonal lattice with a 5.2 Å nearest neighbor separation). Although the bulk crystal lattice has a large mismatch, PbSt monolayers are deposited on hexagonal mica substrate in a well-defined orientation, such that there is a close match between one set of strained lattice rows and the substrate. However, the other lattice constants of the monolayer are not as highly strained and are far from commensurate with the substrate (*38*). In spite of this large mismatch, PbSt monolayers have long-range positional and orientational order. The orientational epitaxy is similar to what is called van der Waals epitaxy, observed in films of transition metal dichalcogenides such as $MoSe_2$ and $NbSe_2$ on mica substrates (*59*). In these films, the adsorbed layer is oriented with the substrate and has long-range order, but even submonolayers maintain the bulk lattice spacings, which can be quite different than those of the substrate. This van der Waals epitaxy is common to layer-forming adsorbates and substrates with strong intralayer interactions but weak and nonspecific interlayer interactions (*59*). For most LB multilayer films, the growth after the first monolayer appears to be primarily van der Waals–type epitaxy. For Pb and Mn, the growth is a combination of strained layer and van der Waals epitaxy on mica.

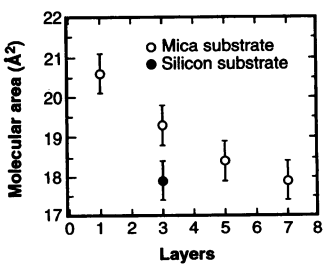

Fig. 8. Interfacial area of $PbSt_2$ films as a function of proximity to a mica (open circles) and silicon (closed circle) substrate. The strain in the lattice is appreciable (on the order of 15% in the area) for the monolayer on the substrate but relaxes to the bulk lattice area by the seventh layer.

Monolayer ordering can be explained by the stronger intralayer interactions for Pb fatty acid salts as opposed to the other counterions. The binding of Pb ions to fatty acid monolayers is complete by pH 4.5, whereas complete binding is not achieved for Cd until pH 6.5 and for Ba until pH 9 (*48, 50*). Langmuir monolayers of Pb fatty acid salts also show greater surface viscosity and elasticity than do Cd fatty acid salts, which suggests again that the intralayer interactions are stronger (*48*). These stronger intralayer interactions in Pb salts help hold the monolayer together, despite the large mismatch between the fatty acid lattice and the substrate lattice. Manganese fatty acid salts must be intermediate between those of Cd and Pb. The best ordering in LB films in general might be achieved by the design of molecules to maximize intralayer interactions while minimizing interlayer interactions (*42*), while the films are simultaneously coupled to a substrate with similar lattice symmetry.

Buckling Modulations and Other Defects

In addition to the herringbone or triclinic lattice structures, the FTs of Cd, Mn, Ba, Ca, and Mg films show additional reflections corresponding to a superstructure within the film. For Cd and Mn counterions, this superstructure is a periodic height modulation with a wavelength of ~1.9 nm in CdA_2 and ~1.2 nm for MnA_2 in the [10] or next-nearest neighbor direction (*18, 23, 37*) (Fig. 3). However, the modulation is not commensurate with the underlying lattice, although the direction is consistent with one of the lattice directions. No such height modulation was observed for Pb multilayers. The simplest explanation of

the modulation is that the counterion interfacial density does not perfectly match the best close-packed alkane lattice. Theory suggests that the modulations can alter the local alkane density to be more compatible with the constraint imposed by the counterion (*40*, *60*). However, the wavelength of the height modulation is only very weakly independent of the length of the alkane chain for a given cation (*37*), in contradiction to the theories based on a competition between preferred head group and tail group spacings that predict a linear dependence (*60*). The theories, however, assume a continuous distribution of allowed tilt angles (*60*), whereas the preferred alkane packing has distinct preferences for angles that preserve the close packing of the chains (*40*, *44*, *52*). The theories also assume no preferred direction for the buckling; we observe that the buckling always occurs along the [10] or next-nearest neighbor direction. The only system in which we have not observed any type of modulation is $PbSt_2$ films, most likely because the Pb ions are so efficient at condensing the lattice that the alkane chains actually occupy a larger interfacial area than do the counterions.

For the triclinic packings of BaA_2 (*36*) (Fig. 4A), CaA_2 (*39*) (Fig. 5A), and $MgSt_2$ (Fig. 6A) films, the superstructures are commensurate with the molecular lattice. That is, the FTs show that the reflections corresponding to the distance between molecular rows is exactly the third, fourth, or second harmonic, respectively, of the reflection corresponding to the superstructure periodicity. Although the local packing is consistent with the ideal triclinic lattice, the superstructure suggests that there are regular defects in this packing. In each case, the unit cell is constructed by the insertion of a regular series of packing defects into one of the ideal triclinic structures. The defects are related to the packing by mirror symmetry (the triclinic is a chiral packing). The defects also contain a component along the chain direction and so serve to alter the interfacial density and tilt angle from those of the uniform triclinic structure. For example, if the BaA_2 film had no defects, the molecular area would be 21.1 $Å^2$ {Kitagorodskii's *T* [1/2 1]} (*50*); the defects reduce the area to 20.4 $Å^2$. Similarly, the defects in the CaA_2 film increase the molecular area from 18.9 $Å^2$ {*T* [1/2 0]} to 19.7 $Å^2$, and the area in the Mg films is decreased from 18.9 $Å^2$ {*T* [1/2 0]} to 18.7 $Å^2$ by the defects. However, the defects do not sacrifice any of the favorable van der Waals energy between alkyl chains because they are simply the mirror image of the normal packing. Instead, the defects allow the alkane lattice to match the interfacial density imposed by the counterions as efficiently as possible.

Stability of LB Films

Another important question regarding the applications of LB films is their long-term stability in various environments. While no significant structural effects on the local lattice structure or on the number of defects are observed when films are aged in laboratory air over the course of several months, significant reorganization occurs when films are aged under water for periods of minutes to hours (*20*). The strength of the head group–head group interaction must be considered as a possible driving force for the reorganization seen in Fig. 9 for cadmium palmitate and cadmium behenate multilayer films. For the shorter palmitate molecules, the entire film has become involved in the reorganization, even after only 10 min of exposure to water. Small bilayer sections simply peeled off the first monolayer ("dewetted") and flipped over onto already covered areas of the film to form multilayer patches (Fig. 9A). The sizes and shapes of the holes in the film are roughly consistent with the sizes and shapes of the multilayer regions. For the longer behenate molecules, exposure to the subphase for the same period of time induces only a few small eruptions and pinholes (Fig. 9B). The reorganization is not simply entropic [as is the case for thermal crystal roughening (*61*)], because the structure of the system appears to approach thick, but flat, crystallites.

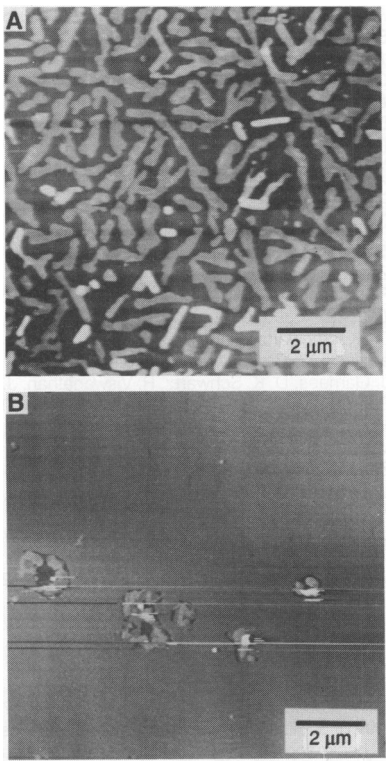

Fig. 9. Atomic force microscopy images (12 μm by 12 μm) of LB films of (**A**) cadmium palmitate (C_{16}) and (**B**) cadmium behenate (C_{22}) after being aged for 10 min under water. In (A), the previously uniform five-layer films have been thoroughly disrupted and have reorganized into small multilayer islands. In (B), the reorganization is much slower—all that is visible are isolated eruption sites that indicate the first stages of the layer folding. The cadmium head group seems to prefer contact with another cadmium head group as opposed to water or the substrate (*61*). Opposing the reorganization are the island edges that have a repulsive interaction between the exposed alkyl chains and water. From (A), it is clear that the cost of edges is not isotropic; the large shape anisotropy of the crystallites suggests that the [01] direction (when in contact with water) is preferred to all others. The increased edge energy of the behenate (B) relative to palmitate (A) also suggests that the kinetics of the reorganization are governed by the costs of the edges.

By stacking higher, the film can increase the number of internal layers while minimizing both substrate and surface interactions. In effect, the cadmium head group prefers to "wet" itself rather than water or substrate (*62*). The energetic penalty is the island edges that have a repulsive interaction between the exposed alkyl chains and water. From the images, it is clear that the cost of edges is not uniform; the large shape anisotropy of the crystallites suggests that the [01] direction is preferred to all others. This edge energy serves to explain, however, why both nucleation and crystal growth take place by the movement and folding of areas large in comparison to molecular dimensions. The ratio of surface area to edges is roughly proportional to the square root of the surface area. Hence, the edge energy for a small island would be disproportionately large. As a consequence, there is likely a minimum-sized island required to initiate folding and nucleate the reorganization, similar to the case in three dimensions for the condensation of a liquid from its vapor stage (*62*).

Changing the length of the hydrocarbon chain, and hence the edge energy, alters the kinetics of the reorganization. After only a few minutes of aging, cadmium palmitate (16 carbons) reached a degree of reorganization comparable to a 30-min-old cadmium arachidate (20 carbons) film. Cadmium behenate (22 carbons) needed ~60 min of aging to reach the stage of first nucleation that was seen in cadmium arachidate after 10 min of aging. Decreasing the edge energy by decreasing the length of the fatty acid hydrocarbon chain clearly decreases the minimum size of a nucleation site, resulting in the faster kinetics. As a practical matter for applications, the longer the alkane chain, the more stable is the film to this type of reorganization (*20*). However, longer chains have drawbacks as well: They form more viscous monolayers and are more difficult to transfer to substrates successfully, although deposition at higher temperatures alleviates many of these problems.

Conclusions

Langmuir-Blodgett films have been touted for their possible applications since the 1930s, many interesting test devices have been made, and even more have been proposed (*1–8*). Still, many of the same basic problems remain: reproducibility, nondestructive testing and characterization, and a fundamental understanding of what controls molecular order and organization in condensed phases. However, these fundamental problems, intractable for the first 60 years of LB film's existence, can now be much more successfully approached with the use of modern spectroscopy and x-ray and scanning probe microscopy techniques. As in MBE, CVD, and the other new materials technologies, the first step is to establish a set of empirical rules concerning such variables as process conditions and substrate choice and treatment for a given film and film application. As such rules develop along with the materials, the fundamental reasons behind the rules will begin to emerge and the process will be put into the realm of science rather than technology. Langmuir-Blodgett technology is certainly just beginning to develop a set of process rules, although studies of these films have taken place for over 60 years. Future device applications of LB films depend on good characterization of substrates and films at the molecular level. Perhaps even more important is how to make best use of the wide variety of variables, such as lattice structures, positional and orientational ordering, and the coupling and decoupling of layers from each other and from the substrate, that have already been observed.

REFERENCES AND NOTES

1. G. G. Roberts, *Langmuir-Blodgett Films* (Plenum, New York, 1990).
2. A. Ulman, *An Introduction to Ultrathin Organic Films* (Academic Press, Boston, MA, 1991).
3. H. Tachibana and M. Matsumoto, *Adv. Mater.* **5**, 796 (1993); C. Pearson, J. E. Gibson, A. J. Moore, M. R. Bryce, M. C. Petty, *Electron. Lett.* **29**, 1377 (1993).
4. J. D. Swalen *et al.*, *Langmuir* **3**, 932 (1987); G. M. Whitesides, J. P. Mathias, C. T. Seto, *Science* **254**, 1312 (1991).
5. S. A. Darst, H. O. Ribi, D. W. Pierce, R. D. Kornberg, *J. Mol. Biol.* **203**, 269 (1988); H. O. Ribi, D. S. Ludwig, K. L. Mercer, G. K. Schoolnik, R. D. Kornberg, *Science* **239**, 1272 (1988).
6. J. K. Pike, H. Byrd, A. A. Morrone, D. R. Talham, *J. Am. Chem. Soc.* **115**, 8497 (1993).
7. S. Mann *et al.*, *Science* **261**, 1286 (1993).
8. A. Monnier *et al.*, *ibid.*, p. 1299.
9. F. Leveiller *et al.*, *ibid.* **252**, 1532 (1991); M. L. Schlossman *et al.*, *Phys. Rev. Lett.* **66**, 1599 (1991); D. K. Schwartz, M. L. Schlossman, P. S. Pershan, *J. Chem. Phys.* **96**, 2356 (1992); K. Kjaer, J. Als-Nielsen, C. A. Helm, L. A. Laxhuber, H. Möhwald, *Phys. Rev. Lett.* **58**, 2224 (1987).
10. H. M. McConnell, *Annu. Rev. Phys. Chem.* **42**, 171 (1991); C. M. Knobler, *Adv. Chem. Phys.* **77**, 398 (1990); H. Möhwald, *Annu. Rev. Phys. Chem.* **41**, 441 (1991).
11. S. Hénon and J. Meunier, *Rev. Sci. Instrum.* **62**, 936 (1991); D. Hönig, G. A. Overbeck, D. Möbius, *Adv. Mater.* **4**, 419 (1992); S. Siegel, D. Hönig, D. Vollhardt, D. Möbius, *J. Phys. Chem.* **96**, 8157 (1992).
12. A. Bonnerot, P. A. Chollet, H. Frisby, M. Hoclet, *J. Chem. Phys.* **87**, 365 (1985); S. Garoff, H. W. Deckman, J. H. Dunsmuir, M. S. Alvarez, *J. Phys.* **47**, 701 (1986); C. Böhm, R. Seitz, H. Riegler, *Thin Solid Films* **178**, 511 (1989); I. R. Peterson, R. Seitz, H. Krug, I. Voigt-Martin, *J. Phys. (France)* **51**, 1003 (1990); B. K. Vainshtein and V. V. Klechkovskaya, *Proc. R. Soc. London A* **442**, 73 (1993); J. Majewski *et al.*, *Science* **261**, 899 (1993).
13. M. Prakash, P. Dutta, J. B. Ketterson, B. M. Abraham, *Chem. Phys. Lett.* **111**, 395 (1984); M. C. Shih, J. B. Peng, K. G. Huang, P. Dutta, *Langmuir* **9**, 776 (1993); J. M. Mikrut, P. Dutta, J. B. Ketterson, R. C. MacDonald, *Phys. Rev. B* **48**, 14479 (1993).
14. P. Tippmann-Krayer, R. M. Kenn, H. Möhwald, *Thin Solid Films* **210**, 577 (1992).
15. R. F. Fischetti, V. Skita, A. F. Garito, J. K. Blasie, *Phys. Rev. B* **37**, 4788 (1988); S. Xu, A. Murphy, S. M. Amador, J. K. Blasie, *J. Phys. I (France)* **1**, 1131 (1991).
16. G. Binnig, C. F. Quate, Ch. Gerber, *Phys. Rev. Lett.* **56**, 930 (1986).
17. D. Rugar and P. K. Hansma, *Phys. Today* **43**, 23 (1990).
18. M. Radmacher, R. W. Tillmann, M. Fritz, H. E. Gaub, *Science* **257**, 1900 (1992).
19. D. K. Schwartz, J. Garnaes, R. Viswanathan, J. A. N. Zasadzinski, *ibid.*, p. 508; D. K. Schwartz, J. Garnaes, R. Viswanathan, S. Chiruvolu, J. A. Zasadzinski, *Phys. Rev. E* **47**, 452 (1993); M. Flörsheimer, A. J. Steinfort, P. Günter, *Surf. Sci. Lett.* **297**, L39 (1993).
20. D. K. Schwartz, R. Viswanathan, J. A. N. Zasadzinski, *J. Phys. Chem.* **96**, 10444 (1992).
21. J. Garnaes, D. K. Schwartz, R. Viswanathan, J. A. Zasadzinski, *J. Synthetic Metals* **57**, 3795 (1993).
22. H. G. Hansma *et al.*, *Langmuir* **7**, 1051 (1991); R. Viswanathan, D. K. Schwartz, J. Garnaes, J. A. N. Zasadzinski, *ibid.* **8**, 1603 (1992).
23. J. Garnaes, D. K. Schwartz, R. Viswanathan, J. A. N. Zasadzinski, *Nature* **357**, 5 (1992).
24. L. Bourdieu, P. Silberzan, D. Chatenay, *Phys. Rev. Lett.* **67**, 2029 (1991).
25. J. Frommer, *Angew. Chem. Int. Ed. Engl.* **31**, 1298 (1992).
26. L. F. Chi, M. Anders, H. Fuchs, R. R. Johnston, H. Ringsdorf, *Science* **259**, 213 (1993).
27. M. Egger *et al.*, *J. Struct. Biol.* **103**, 89 (1990); A. L. Weisenhorn *et al.*, *Langmuir* **7**, 8 (1991).
28. J. A. Zasadzinski *et al.*, *Biophys. J.* **59**, 755 (1991); S. Hui, R. Viswanathan, J. A. Zasadzinski, D. Leckband, J. Israelachvili, unpublished data.
29. V. V. Tsukruk, D. H. Reneker, H. Bengs, H. Ringsdorf, *Langmuir* **9**, 2141 (1993); V. V. Tsukruk, M. D. Foster, D. H. Reneker, A. Schmidt, W. Knoll, *ibid.*, p. 3538.
30. J. P. K. Peltonen, P. He, J. B. Rosenholm, *J. Am. Chem. Soc.* **114**, 7637 (1992); *Langmuir* **9**, 2363 (1993).
31. O. Marti *et al.*, *Science* **239**, 50 (1988); C. A. J. Putnam, H. G. Hansma, H. E. Gaub, P. K. Hansma, *Langmuir* **8**, 3014 (1992); B. M. Goettgens, R. W. Tillmann, M. Radmacher, H. E. Gaub, *ibid.*, p. 1768.
32. J. Y. Josefowicz *et al.*, *Science* **260**, 323 (1993).
33. J. Garnaes *et al.*, unpublished data.
34. C. J. Eckhardt *et al.*, *Nature* **362**, 614 (1993).
35. E. Meyer *et al.*, *ibid.* **349**, 398 (1991).
36. D. K. Schwartz, R. Viswanathan, J. A. N. Zasadzinski, *Phys. Rev. Lett.* **70**, 1267 (1993); *Langmuir* **9**, 1384 (1993).
37. D. K. Schwartz, R. Viswanathan, J. Garnaes, J. A. Zasadzinski, *J. Am. Chem. Soc.* **115**, 7374 (1993).
38. R. Viswanathan, J. A. Zasadzinski, D. K. Schwartz, *Science* **261**, 449 (1993).
39. ———, *Nature*, in press.
40. D. K. Schwartz, C. M. Knobler, R. Viswanathan, J. A. Zasadzinski, in preparation.
41. E. Meyer *et al.*, *Phys. Rev. Lett.* **69**, 1777 (1992); R. M. Overney *et al.*, *Nature* **359**, 133 (1992).
42. H. E. Ries Jr., *Sci. Am.* **204**, 152 (March 1961); ———, M. Matsumoto, N. Uyeda, E. Suito, *Adv. Chem. Ser.* **144**, 286 (1975); *J. Colloid. Interface Sci.* **57**, 396 (1976); J. R. Fryer, R. A. Hann, B. L. Eyres, *Nature* **313**, 382 (1985); N. Uyeda, T. Takenaka, K. Aoyama, M. Matsumoto, Y. Fujiyoshi, *ibid.* **327**, 319 (1987); S. Y. Luk, A. C. Wright, J. O. Williams, *Thin Solid Films* **186**, 147 (1990).
43. C. J. Eckhardt *et al.*, *Langmuir* **8**, 2591 (1992); C. J. Eckhardt and D. R. Swanson, *Chem. Phys. Lett.* **194**, 370 (1992).
44. A. I. Kitaigorodskii, *Organic Chemical Crystallography* (Consultant Bureau, New York, 1961).
45. S. Karaborni, S. Toxvaerd, O. H. Olsen, *J. Chem. Phys.* **96**, 4965 (1992); J. P. Bareman, G. Cardini, M. L. Klein, *Phys. Rev. Lett.* **60**, 2152 (1988).
46. Y. Shnidman, A. Ulman, J. E. Eilers, *Langmuir* **9**, 1071 (1993).
47. L. Pauling, *The Nature of the Chemical Bond* (Cornell Univ. Press, Ithaca, NY, ed. 3, 1960), p. 43.
48. M. Yazdanian, H. Yu, G. Zografi, *Langmuir* **6**, 1093 (1990); ———, M. W. Kim, *ibid.* **8**, 630 (1992).
49. This tendency to form mixed protonated and deprotonated fatty acid films at low pH was the basis for one of the first patents on LB films by Blodgett. Protonated films are soluble in a number of organic solvents, whereas the metal salts are not. By control of the pH, it is possible to remove a fraction of the LB film selectively, a process called skeletonization by Blodgett. These films were used to create low reflection coatings on glass surfaces by providing a low refractive index material on both sides of the glass. Unfortunately, as has been the case for many LB film applications, the method was not practical, because the films were removed by even gentle wiping.
50. K. Kobayashi, K. Takaoka, S. Ochiai, *Thin Solid Films* **159**, 267 (1988); B. P. Binks, *Adv. Colloid Interface Sci.* **34**, 343 (1991); D. J. Ahn and E. I. Franses, *J. Chem. Phys.* **95**, 8486 (1991).
51. A. Bonnerot, P. A. Chollet, H. Frisby, M. Hoclet, *J. Chem. Phys.* **87**, 365 (1985).
52. D. A. Outka, J. Stöhr, J. P. Rabe, J. D. Swalen, H. H. Rotermund, *Phys. Rev. Lett.* **59**, 1321 (1987).
53. Behenic [$CH_3(CH_2)_{20}COOH$], arachidic [$CH_3(CH_2)_{18}COOH$], stearic [$CH_3(CH_2)_{16}COOH$], and palmitic [$CH_3(CH_2)_{14}COOH$] acids were spread from chloroform solution (1.7 to 2.0 mg/ml) onto an aqueous subphase in a commercial Langmuir-Blodgett trough (NIMA Technology, Coventry, England). The cations were added to the subphase as 0.5 mM solutions of $CdCl_2$, $MnCl_2$, $BaCl_2$, $CaCl_2$, $MgCl_2$, $ZnCl_2$, or $Pb(CH_3COO)_2$, and the solution pH was adjusted either to between 6.5 and 7 (for BaA_2, MnA_2, and CdA_2) by the addition of $NaHCO_3$ or to 7.0 ($PbSt_2$, $CaCl_2$, $ZnCl_2$, and $MgCl_2$) by the addition of NaOH. The respective pHs were chosen by the criterion that the isotherm should contain no trace of the "liquid-condensed" phase that exists at lower pH, which correlates well with full complexation of the metal salt (*48, 53, 57*). Alkaline earth metals such as Ba, Ca, and Mg require significantly higher pHs for full complexation. However, BaA_2, $CaCl_2$, and $MgCl_2$ multilayers prepared from films with pH > 9 showed no difference in macroscopic or microscopic structure from the films prepared at pH 7, which is in agreement with other data in the literature (*48, 53, 57*). In general, we observed no changes in the structures of any of the films with increasing pH, once the liquid-condensed phase was absent from the isotherms (*48*). The area per molecule for all species at this surface pressure was in the range of 18 to 20 Å^2 per molecule; there was no correlation between the area per molecule on the trough (relative error of ±5%) and the structures we observed on the transferred films. Film transfer was by vertical dipping at approximately 2.0 mm/min; transfer ratios were approximately unity. Substrates were either freshly cleaved mica or silicon wafers polished on both sides [orientation, (100); 3 to 5 ohm·cm; *n*-type; ~0.4 mm thick] with a root-mean-square roughness of approximately 2 Å as measured by AFM (Semiconductor Pro-

cessing, Boston). The AFM measurements were performed with a Nanoscope III FM (Digital Instruments) at ambient temperature. A 1 μm by 1 μm scan head and a silicon nitride tip on a cantilever with a spring constant of 0.12 N/m were used. The best molecular resolution was achieved in the "force" mode, that is, by scanning the tip at constant height and measuring spring deflection. Lighter colors correspond to higher areas in the images. Typical forces were 10^{-8} N.

54. The approximate tilt angle is given by $\tan \theta = nR/D$, where R is the next nearest carbon spacing in the all trans chain, 2.52 Å; D is the separation between molecules, about 4.5 Å for nearest neighbors and 7.5 Å for next-nearest neighbors in our close-packed systems; and n is an integer. For the nearest neighbors, the first tilt is approximately 30°; for next-nearest neighbors, the first tilt is about 19°.
55. L. Bourdieu, O. Ronsin, D. Chatenay, *Science* **259**, 798 (1993).
56. X. Qui, J. Ruiz-Garcia, K. J. Stine, C. M. Knobler, J. V. Selinger, *Phys. Rev. Lett.* **67**, 703 (1991); J. V. Selinger, Z.-G. Wang, R. F. Bruinsma, C. M. Knobler, *ibid.* **70**, 1139 (1993).
57. C. Vogel, J. Corset, M. Dupeyrat, *J. Chim. Phys.* **76**, 909 (1979).
58. E. B. Sirota, H. E. King Jr., D. M. Singer, H. S. Shao, *J. Chem. Phys.* **98**, 5809 (1993); E. B. Sirota, H. E. King Jr., G. J. Hughes, W. K. Wan, *Phys. Rev. Lett.* **68**, 492 (1992).
59. K. Ueno, K. Saiki, T. Shimada, A. Koma, *J. Vaccine Sci. Technol. A* **8**, 68 (1990); A. Koma, K. Saiki, Y. Sato, *Appl. Surf. Sci.* **41/42**, 451 (1989); F. S. Ohuchi, B. A. Parkinson, K. Ueno, A. Koma, *J. Appl. Phys.* **68**, 2168 (1990).
60. J. M. Carlson and J. P. Sethna, *Phys. Rev. A* **36**, 3359 (1987); S. A. Safran, M. O. Robbins, S. Garoff, *ibid.* **33**, 2186 (1986).
61. M. Wortis, in *Chemistry and Physics of Solid Surfaces VII*, R. Vanselow and R. Howe, Eds. (Springer-Verlag, Berlin, 1988), pp. 367–405.
62. J. N. Israelachvili, *Intermolecular and Surface Forces* (Academic Press, London, 1992), vol. 2.
63. J.A.Z. thanks J. Israelachvili, C. M. Knobler, H. Yu, G. Zografi, S. Hui, and S. Mann for useful discussions on LB films. We especially thank P. Hansma and his group for a thorough introduction to probe microscopy and F. Grunfeld of NIMA Technologies and V. Elings of Digital Instruments for assistance with instrumentation. Supported by the Office of Naval Research under grant N00014-90-J-1551; the National Science Foundation under grants CTS90-15537, CTS-9212790, and CHE89-02354 (D.K.S. through C. Knobler); the National Institutes of Health under grant GM 47334; and the Donors of the Petroleum Research Foundation.